NUMERICAL STUDY OF COMBINED MODULATED ELECTROMAGNETIC WAVE PARAMETERS IN FORWARD MODELING OF REFLECTED SEISMIC WAVES FROM SUBSURFACE LAYERS

MARYAM NOROOZI[1], MOHAMAD ALI RIAHI[1] and ALI BOSTANI [2]

[1] Institute of Geophysics. University of Tehran, Tehran, Iran.
[2] CEO at BEM Technology Group, Tehran, Iran.
noroozi.maryam@ut.ac.ir, mariahi@ut.ac.ir, a.bostani@bem-tech.com

(Received May 3, 2023; accepted July 5, 2023)

ABSTRACT

Noroozi, M., Riahi, M.A. and Bostani, A., 2023. Numerical study of combined modulated electromagnetic wave parameters in forward modeling of reflected seismic waves from subsurface layers. *Journal of Seismic Exploration*, 32: 357-372.

Nowadays, a combination of different methods are implemented for identifying subsurface reserves with the aim of increasing accuracy and reducing failure costs. In exploration geophysics, electromagnetic methods with a controlled source are used in land and sea environments to study subsurface structures. On the other hand, seismic methods are traditionally the most common method for hydrocarbon explorations. In this study, a combination of the two methods is used.

As usual for solving electromagnetic wave equations, the dielectric coefficient parameter is assumed to be constant. But here the electromagnetic wave equations are solved by considering the dielectric coefficient parameter, resulting in a higher accuracy in identifying the subsurface layers.

The importance of the dielectric coefficient parameter is that the value of this parameter for oil and gas with its value for the host rock surrounding the oil and gas trap is significantly different, therefore it facilitates the exploration process.

Also in our numerical modeling, we used a wave packet which includes a sinusoidal wave and a square wave that is propagated into the Earth model in a modulated form. Those waves have different wavelengths because waves with long wavelengths can penetrate deeper while waves with short wavelengths result in more resolution.

0963-0651/23/$5.00

We used the Marmousi2 model which is made up of several hydrocarbon sections including the Marmousi hydrocarbon section. Then, using the empirical relationship between seismic velocity and the resistivity parameter we extracted the dielectric coefficient parameter. According to the lithological information we produced a dielectric coefficient matrix. Finally, with this information, we made a numerical forward modeling code to generate the final output of this model which is the intensity of the ground-induced reflected fields received by the receivers. Then a forward model for the seismological method was prepared and the output related to the reflection coefficient was obtained for this model.

The comparison of these two outputs with 3 methods, consisting of the mean squared error, structural similarity index, and histogram chart. we observe that when using the joint method, the results of the properties of the layers are obtained more accurately than when using the conventional seismic method alone.

KEY WORDS: seismic method, electromagnetic method, dielectric coefficient, Marmousi2 model, reflection coefficient, mean squared error, structural similarity index.

INTRODUCTION

The use of electromagnetic and seismic methods provides additional information about the resistivity and velocity of subsurface structures. Seismic reflection is a highly effective tool for imaging structures in sedimentary basins for hydrocarbon exploration. However, in a hard rock environment, the quality of seismic data can severely diminish. For example, suboptimal survey parameters, steeply dipping structures, near-surface volcanic rocks, extreme topography and variations in weathering layer thickness, complex near-surface velocity variations, or the presence of high-velocity rocks above low-velocity layers can degrade the quality of seismic data due to insufficient wave penetration, scattering, multiples, and static effects. On the other hand, the presence of high-velocity layers over low-velocity layers is generally associated with corresponding high electrical resistivity over low resistivity, which is favorable for structural imaging using MT or EM data (Takougang et al., 2015). Also, Because of the long wavelengths used in the seismic method, the resolution is low. It also occurs when the impedance (the product of density multiplied by the amount of velocity) used to separate the subsurface layers becomes degenerative. Indeed, there are two adjacent layers, each with its velocity and density, but the product of their multiplication is the same, so we make a mistake in interpreting the separation of the layers because we have more than one answer for the conditions of an equation. On the other hand, sometimes an environment becomes an absorbent medium due to its high porosity, which means seismic waves cannot pass through it, or if they do, their energy is so weakened in the reflection so high priority in the layers will cause sharp

damping in the amplitude of the reflection and the result is that the reflection is so weak that it is in the noise domain so it cannot be detected.

The seismic method has all of the problems above. But, there are different methods to solve them. In this research, a new method in the field of electromagnetism has been used to improve the response of subsurface structures.

As usual for solving electromagnetic wave equations, the dielectric coefficient parameter is assumed to be constant. But here the electromagnetic wave equations are solved by considering the dielectric coefficient a parameter, resulting in higher accuracy in separating the subsurface layers (Bostani, 2020). The importance of this parameter is that the value of this parameter for oil and gas with the value of it for the bedrock around the oil and gas is significantly different, therefore it facilitates the exploration process. Also in our model, we used a wave packet that includes a sinusoidal wave and a square wave that is sent to Earth in a modulated form. Those waves have different wavelengths because waves with a long wavelength can penetrate deeper and waves with a short wavelength can give us more resolution.

In this study, synthetic data from the Marmousi2 model have been used (Martin, 2004). The reasons for using synthetic data are that first of all, synthetic data provide more details in terms of lithology; and secondly, given the fact that the proposed method is a new topic. Therefore, we initially started to consider the reliability results of this integration using synthetic data.

Martin (2004) created the Marmousi2 model by first reconstructing the original Marmousi model by using GX Technology Corporation's GXII modeling software, which allows the construction of 2D models from segments of horizons. The original Marmousi model was an acoustic model. It possessed compressional wave velocities (P-wave velocities) and densities (ρ). The Marmousi2 model is elastic and therefore must also possess shear wave velocities (S-wave velocity). He determined the layer properties based on the Marmousi P-wave velocity and an assigned lithology. Marmousi2 model has been produced with a profile length of 17 km and a depth of 3500 meters. The structural elements of Marmousi2 are shown in Fig. 1. This figure shows the model horizons and P-wave velocity.

He introduced additional horizons to create new locations in which to insert hydrocarbons into the model. These are shown as red (gas) and green (oil) in Fig. 3. They are distributed within the complex faulted zone at different depths, and also in the simple structure at the flanks. These layers vary in size, shape, and structural complexity.

Not all Marmousi2 data were used in this study, but some of the mentioned data were examined. Because the size of the matrices was large and the amount of data was huge so the production of the dielectric coefficient matrix was very time-consuming. On the other hand, to show that the output of the combined method in the hydrocarbon range is more accurate than the seismic method, part of this matrix was selected to cover the two hydrocarbon ranges. The selected Marmousi2 model has a profile length of 8 km and a depth of 3000 meters. The P-wave velocity diagram for the study range is shown in Fig. 2.

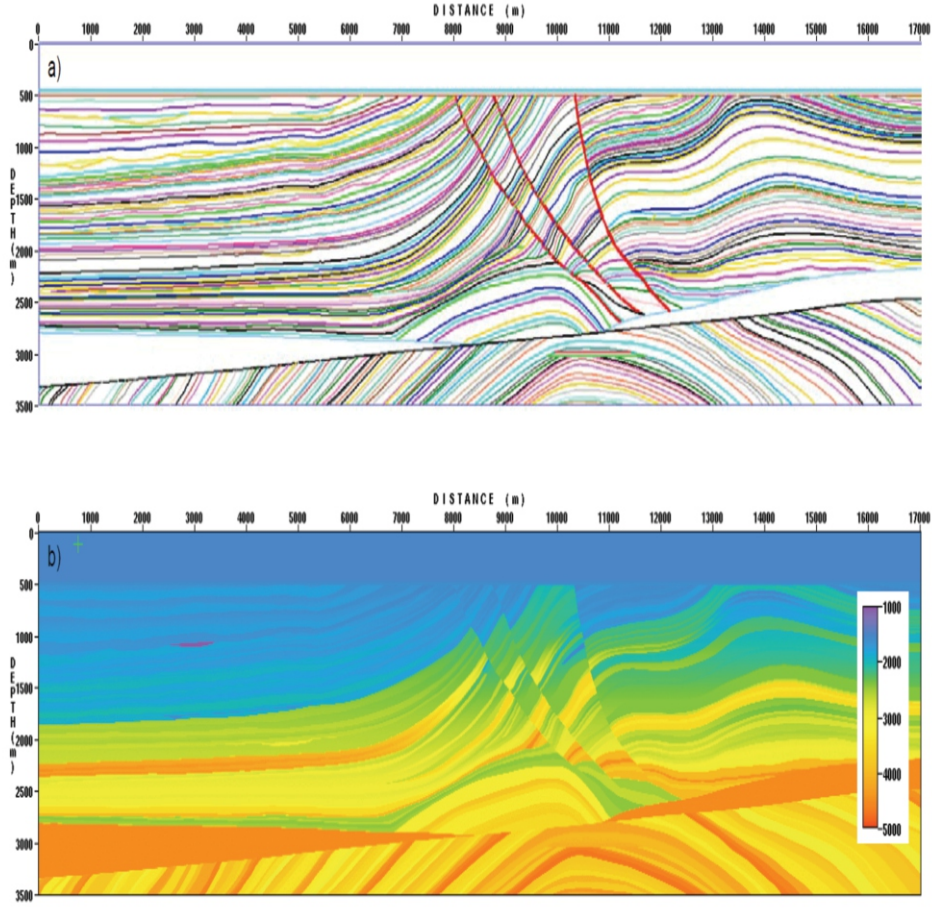

Fig. 1. Marmousi2. a) Model horizons, b) P-wave velocity (Martin, 2004).

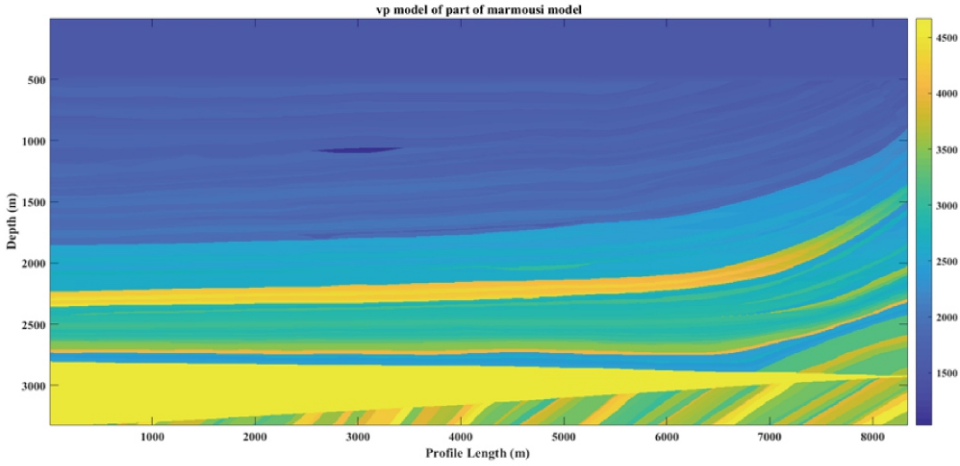

Fig. 2. The P-wave velocity diagram for the study range.

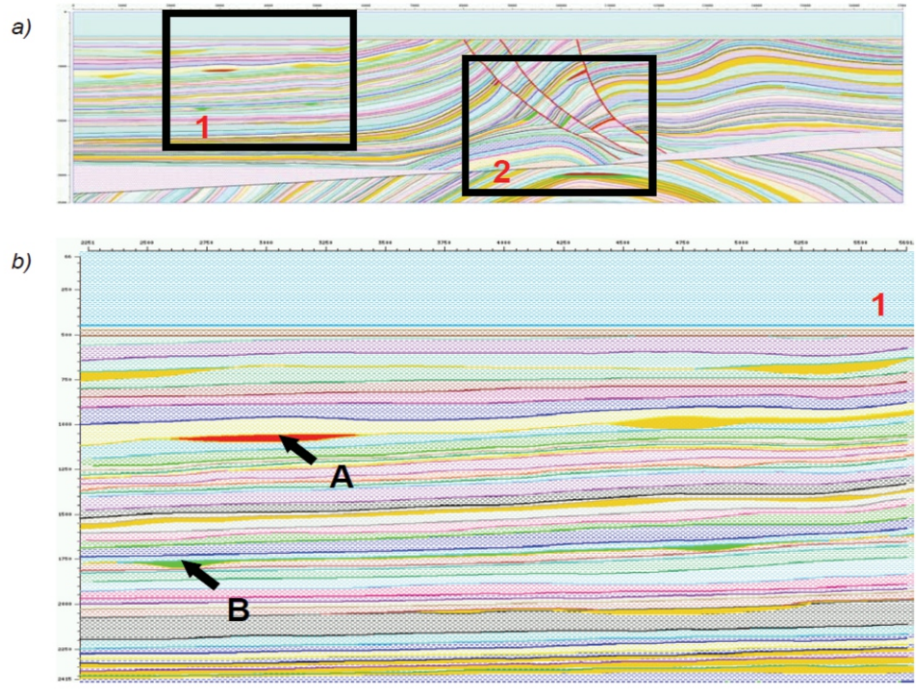

Fig. 3. Hydrocarbon units. a) Overview shows the location of hydrocarbon units, b) location of hydrocarbon area 1 shown in greater detail, in which red area represents gas and green area represents oil (Martin, 2004).

In the following, first, the type of electromagnetic wave used in this method is explained and then a relation for combining the two methods of EM and seismic is expressed. Finally, a comparison of the output of the seismic forwards model and the combined forward model is given.

METHOD AND/OR THEORY

Electromagnetic Wave Equation

We send two waves of different wavelengths inside the Earth and receive two reflections. Consider a single sine wave with a square wave pack. We define the equation of the sum of these two waves as follows:

$$H = H_0[square(\omega_1 t) + \sin(\omega_2 t)] \quad , \tag{1}$$

where ω_1 indicates a low frequency of the order of 10 Hz and less, and ω_2 indicates a high frequency of the order of 100 kHz to 10 kHz. H represents the pure magnetic field that is sent. In the relation above, the square wave can be written as follows:

$$square\ (\omega_1 t) = \sum_{n=1}^{\infty} \frac{\sin[(2n-1)\omega t]}{2n-1} \quad . \tag{2}$$

The general form of the wave equation for the new wave defined in eq. (1) is as follows:

$$\nabla^2 H + \mu\varepsilon \frac{\partial^2 H}{\partial t^2} - \mu\sigma \frac{\partial H}{\partial t} = 0 \quad . \tag{3}$$

On a trigonometric plane, each wave can be represented as a vector. According to eq. (1), which is the sum of two waves, this relation can be expressed in a vector. Therefore, according to the principle of superposition, eq. (1) can be rewritten based on the expansion of the base frequency as follows:

$$\nabla^2 H_0 e^{i\omega_1 t} - \omega_1^2 \varepsilon\mu \frac{\partial^2 H_0}{\partial t^2} e^{i\omega_1 t} - i\omega_1 \sigma\mu \frac{\partial H_0}{\partial t} e^{i\omega_1 t} + \nabla^2 H_0 e^{i\omega_2 t} - \omega_2^2 \varepsilon\mu \frac{\partial^2 H_0}{\partial t^2}$$
$$\times\ e^{i\omega_2 t} - i\omega_2 \sigma\mu \frac{\partial H_0}{\partial t} e^{i\omega_2 t} = 0 \quad , \tag{4}$$

Eq. (4) is our new electromagnetic wave equation, now we have to solve this equation. Suppose we have a dipole field in a spatial component:

$$H_0 = \frac{1}{4\pi}\left[-\frac{m}{r^3} + \frac{3(m.r)\vec{r}}{r^5}\right] \quad , \tag{5}$$

where m is defined as follows:

$$\vec{m} = InA\hat{n} \quad .$$

A loop with current I, n number of turns of the coil, and area A. (Jackson, 1998).

Because the transmitted waves have two frequencies with Approximately large frequency intervals, we can say that they act independently, and it is as if we have sent these two waves with different frequencies separately. So we will have:

$$\nabla^2 H_0 e^{i\omega_1 t} - \omega_1^2 \varepsilon\mu \frac{\partial^2 H_0}{\partial t^2} e^{i\omega_1 t} - i\omega_1 \sigma\mu \frac{\partial H_0}{\partial t} e^{i\omega_1 t} = 0 \quad , \tag{6}$$

$$\nabla^2 H_0 e^{i\omega_2 t} - \omega_2^2 \varepsilon\mu \frac{\partial^2 H_0}{\partial t^2} e^{i\omega_2 t} - i\omega_2 \sigma\mu \frac{\partial H_0}{\partial t} e^{i\omega_2 t} = 0 \quad . \tag{7}$$

Solving the two equations above in cylindrical coordinates. The magnetic field is cylindrical and its propagation direction is in the direction of the z-vector. In this case, by expanding the field in the cylindrical coordinates, the field will have three components. We will have a radial component that can be described by the Bessel function. We have a component in the z-direction that gives us an exponential sentence in the z-direction. And finally, we have a component in the direction φ (rotational angle), because we have symmetry on φ, the value of the corresponding exponential sentence becomes one.

According to the above explanations, the answers to eqs. (6) and (7) are as follows:

$$H = H_0 \sum_n A_n J_n(\gamma_n r) e^{-i(\alpha z - \omega t)} \tag{8}$$

In the relation above, to simplify the shape of the equation we defined parameters α and γ as follows:

$$\alpha^2 = i\omega\sigma\mu \quad \& \quad \gamma^2 = \omega^2\varepsilon\mu \quad ,$$

where H_0 represents the initial dipole field and A_n is defined by the boundary conditions. Considering the Bessel function of the first kind we will have:

$$H \cong A_1 J_1(\gamma r) e^{-i\frac{\sqrt{2}}{2}\sqrt{\omega\sigma\mu}z} e^{-\frac{\sqrt{2}}{2}\sqrt{\omega\sigma\mu}z} e^{i\omega t} \quad . \tag{9}$$

The sentence $e^{-\frac{\sqrt{2}}{2}\sqrt{\omega\sigma\mu}z}$ is an attenuation sentence and the two sentences $e^{-i\frac{\sqrt{2}}{2}\sqrt{\omega\sigma\mu}z}$ and $e^{i\omega t}$ are oscillating sentences.

Seismic Wave Equation

When both density and seismic wave velocity are spatially variable, the acoustic wave equation reads:

$$\frac{\partial}{\partial x}\left(\frac{1}{d}\frac{\partial p}{\partial x}\right) + \frac{\partial}{\partial y}\left(\frac{1}{d}\frac{\partial p}{\partial y}\right) = \frac{1}{c^2 d}\ddot{p} + s \quad , \tag{10}$$

where *P(x, y, t)* represent the pressure, *d(x, y)* the density, *c(x, y)* the wave velocity, and *s(x, y, t)* the source term which equals the divergence of the body force divided by the density. In eq. (10) and throughout, a dot above a variable denotes differentiation with respect to time. (Kosloff and Baysal, 1982).

The Fourier method solves eq. (10) by discretization in both space and time. Yielding a discrete approximation to eq. (10) given by

$$LP^n(i,j) = \frac{1}{c^2 d \Delta t^2}\left[P^{n+1}(i,j) - 2P^n(i,j) + P^{n-1}(i,j)\right] + S^n(i,j)\,, \tag{11}$$

where $P^n(i,j,)$ and $S^n(i,j)$, respectively, represent the value of pressure and source at time $t{=}n\Delta t$ and at spatial location $x = x_0 + (i-1)\Delta x$, $y = y_0 + (j-1)\Delta y$. $LP^n(i,j)$ represents the numerical approximation of the left-hand side of eq. (10).

Eq. (11) contains an explicit, second-order, time-differencing scheme similar to schemes often used in finite-difference and finite-element codes. The point of departure for the Fourier method is the manner in which the spatial derivatives are calculated.

The term $LP^n(i,j)$ in eq. (11) is calculated in two separate passes, one for the terms containing x-derivatives and one for the terms containing y-derivatives. In the pass for the x-derivatives, $\frac{\partial}{\partial x}\left(\frac{1}{d}\frac{\partial p}{\partial x}\right)$is calculated for each of the grid lines. Along with each x-line$\frac{\partial p}{\partial x}$ is calculated by first performing a spatial FFT on P. The result is then complex multiplied by the spatial wavenumber vector iK_ν ,ν = 1 ..., N_x, where N_x is the number of grid points

in each x-line and$i = \sqrt{-1}$. This operation is followed by an inverse FFT into the spatial domain yielding $\frac{\partial p}{\partial x}$. In the second stage $\frac{\partial p}{\partial x}$ is multiplied by the vector 1/d, and again a forward and inverse FFT are used to get $\frac{\partial}{\partial x}\left(\frac{1}{d}\frac{\partial p}{\partial x}\right)$. When the calculation has been completed along all the x-lines, a similar process is applied in a second pass to get $\frac{\partial}{\partial y}\left(\frac{1}{d}\frac{\partial p}{\partial y}\right)$ along all the y-line.

Resistivity-Seismic Velocity Relations

Electrical conductivity is created by the passage of electric current through materials with free electrons, such as metals, which is the result of electron polarization, which is caused by an alternating electric field. Electrical conductivity is expressed by the following relation;

$$\sigma = J/E = 1/\rho = L/AR \quad , \tag{12}$$

where J represents electric current density and E represents electric field intensity. The electrical resistivity of a rigid cylinder with length L and cross-section A with the resistance R is expressed by ρ.

Unlike seismic waves, EM waves propagate by diffusion within the earth and cannot provide the same resolution. The resolution of MT data is much lower than that of seismic data. The resolution of standard seismic reflection data is a few tens of meters whereas that of EM data can vary from a few meters to several hundreds of meters, depending on frequency and depth. The shallow part of the subsurface is generally better resolved than the deeper part. As mentioned earlier, the MT data can provide crucial complementary information in complex areas such as sub basalt or subsalt in which imaging using seismic data alone can be very challenging. In this context, the seismic data could be used to obtain the geometry of the upper part of the model, whereas the MT data are used to get the geometry of the sub-basalt or subsalt. (Meju et al., 2003).

We use a velocity V_P-resistivity ρ relationship in the form

$$log_{10} V_P = c(log_{10} \rho)^2 + d\, log_{10} \rho + e \quad . \tag{13}$$

Or in the form (Meju et al., 2003)

$$log_{10} V_P = d\, log_{10} \rho + e \quad , \tag{14}$$

where the coefficients c, d, and e are to be estimated from regression of the velocity and resistivity values obtained from available well logs.

Consider a plane wave, propagating in the material of uniform velocity α_2, that intersects a horizontal interface. α_1, ρ_1, and ρ_2 represent the velocity and density of high and low levels, respectively. Describe the incident wave with function f (t – z /α_1), the reflected wave by g (t + z/α_2), and the transmitted wave by h (t – z /α_2). Where f, g, and h represent arbitrary functions that describe waves. Considering boundary conditions that necessitate continuity of displacement and pressure, reflected and transmitted waves can be described according to the incident wave.

Assuming that the incident wave is propagated at z = 0, so for continuity of displacement will have;

$$f_{z=0} + g_{z=0} = h_{z=0} \tag{15}$$

We use Hooke's law to generate stress boundary conditions. The bulk modulus reads:

$$P(x, t) = -K(x)\, \theta(x, t) \quad . \tag{16}$$

For a heterogeneous liquid, Hooke's law relates the pressure to the negative variation of the differential volume. In the 1D dimension, this relation is reduced to p = −K∂zu where p is the pressure, u is the displacement and K is the bulk modulus. The wave velocity is obtained from the square root of the bulk modulus divided by the density, or its equivalent $K = \rho\alpha^2$. Therefore, the continuity of pressure can be expressed by the following relation:

$$\rho_1 \alpha_1^2 \frac{\partial f}{\partial z} + \rho_1 \alpha_1^2 \frac{\partial g}{\partial z} = \rho_1 \alpha_2^2 \frac{\partial h}{\partial z} \quad , \tag{17}$$

$$\rho_1 \alpha_1 f' + \rho_1 \alpha_1 g' = \rho_1 \alpha_2 h' \quad . \tag{18}$$

By considering the definition of impedance as I = ρα and also considering the relation (15), we can write:

$$\mathrm{Rc} = \frac{I_2 - I_1}{I_2 + I_1} \quad , \quad T = \frac{2I_1}{I_2 + I_1} \quad , \tag{19}$$

where Rc represents the reflection coefficient and T represents the transmission coefficient. To investigate the ground response, we will model the reflection coefficient relationship. The relation Rc* wavelet = s(w), to simulate the ground response we must convolve the reflection coefficient in a wavelet. The Ricker wavelet has zero phases and is the most suitable model for comparison with fully processed seismic images. By considering the velocity model from the Marmousi model data, we obtained the reflection coefficient. The Ricker wavelet is expressed in the form:

$$w(t)_{ricker} = [1 - 2\pi^2 f^2 t^2] e^{-\pi^2 f^2 t^2} \quad . \tag{20}$$

A frequency of 40 Hz and a time interval of [0.1: 0.1-] with a sampling rate of 0.004 s and periodicity of 0.04 s were considered. In the following, a seismic forward model was written to obtain the reflection coefficient related to the Marmousi2 model which was convolved with the Ricker wavelet shown in Fig. 5, and its time domain is shown in Fig. 4.

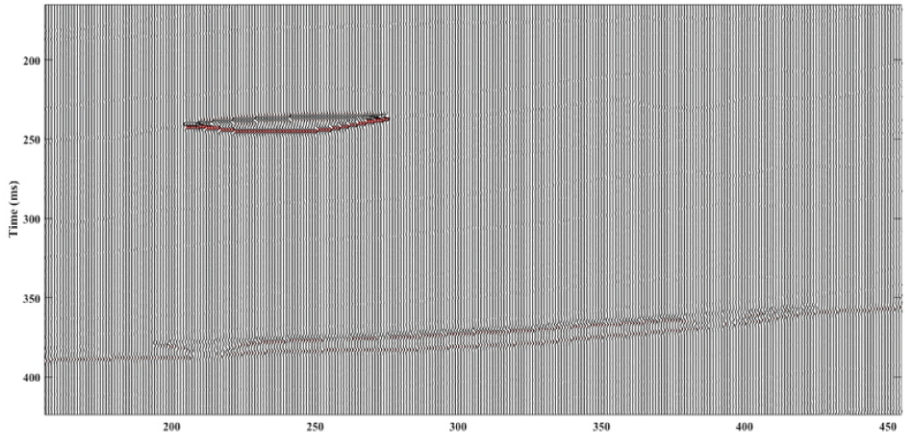

Fig. 4. a) The reflection coefficient was convolved with the Ricker wavelet in the time domain b) location of hydrocarbon is shown in greater detail.

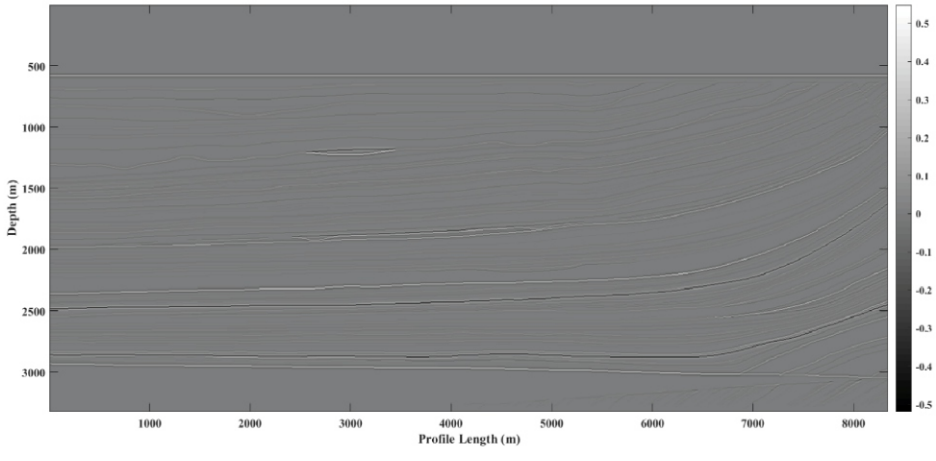

Fig. 5. The reflection coefficient was convolved with the Ricker wavelet (depth).

To create a forward model related to the combined electromagnetic and seismic methods, resistivity and dielectric coefficient matrices were required. According to the information available about the stratigraphy of the earth and also based on eq. (14), resistivity matrices were produced by MATLAB software. Also, the dielectric coefficient matrix was generated according to the stratigraphic structure of the earth. To generate modulated electromagnetic wave a square wave with a frequency of 1200 Hz, with a periodicity of 500 microseconds, which is sent for 5 microseconds, and a sine wave with a periodicity of 2 seconds and a frequency of 10 Hz was used. According to eq. (9), we have obtained the value of the magnetic field and from its spatial derivative, we have obtained the time derivative of the electric field. From the result of the obtained values, the amplitude of the electromagnetic field received in the receiver can be obtained. This result is called the Earth's response to the electromagnetic wave (Fig. 6).

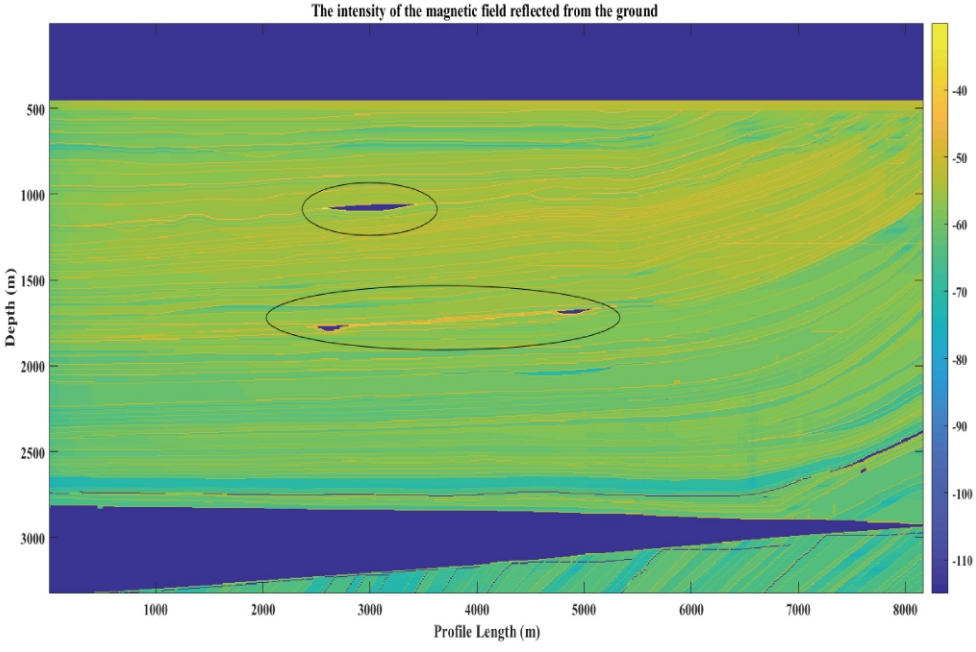

Fig. 6. The intensity of the magnetic field reflected from the ground.

DISCUSSION

Now we must compare two results (Figs. 5 and 6 with Fig. 2). For comparison, we used 3 methods.

Mean Squared Error (MSE)

To compare two images, we use the MSE of the pixel values of the two images. Similar images will have less mean square error value. Here we use Python to compute MSE between our images. We consider the Vp model image (Fig. 2) as the reference image and the intensity of the magnetic field reflected from the ground (Fig. 6) as the image whose pixel values you would like to compare with the first one, and another time we consider the reflection coefficient was convolved with the Ricker wavelet (Fig. 5) as the second image for comparing with p wave model image. After computing MSE, the image-matching error between Fig. 6 and Fig. 2 was 28.339647, and the image-matching error between Fig. 5 and Fig. 2 was 45.843910. So we see the result related to the combined electromagnetic and seismic methods is clearly more similar to the Vp model.

Structural Similarity Index Measure (SSIM)

The Structural Similarity Index Measure (SSIM) is a perceptual metric that quantifies image quality degradation caused by processing such as data compression or by losses in data transmission. It is a full reference metric that requires two images from the same image capture, a reference image, and a processed image. The SSIM values range between 0 to 1, 1 means a perfect match of the reconstructed image with the original one. Again we use Python to compute the value of SSIM for our images. After computing, SSIM for Fig. 6 and Fig. 2 was 0.80373, and the image matching error between Fig. 5 and Fig. 2 was 0.77216. So we see the result related to the combined electromagnetic and seismic methods clearly has more structural similarity to the Vp model.

Histogram chart

A histogram is a graph used to represent the frequency distribution of a few data points of one variable. Here, a histogram is drawn for two hydrocarbon ranges A and B, which are related to gas and oil, respectively with MATLAB. To compare the frequency of hydrocarbon ranges A and B for the P-wave velocity model with the frequency of the reflection coefficient was convolved with the Ricker wavelet and the intensity of the magnetic field reflected from the ground in the combined method. The corresponding values for these variables are given in Table 1. It should be

noted that the values of this table are extracted from the matrix related to the outputs obtained from the forward model.

Table 1. Parameter values for gas and oil ranges.

	gas	oil
Vp model	1028	1640
the reflection coefficient was convolved with the Ricker wavelet	0.3 & - 0.4	0.15 & - 0.16
the intensity of the magnetic field reflected from the ground in the combined method	-45	-40

In Fig. 7, the histogram diagram related to hydrocarbon range A is drawn. As we can see in the figure and according to the values of Table 1, the frequency of gas for the figure of the P-wave model is 397, for the figure of the reflection coefficient was convolved with the Ricker wavelet is 135, and for the figure of the intensity of the magnetic field reflected from the ground in the combined method is 345.

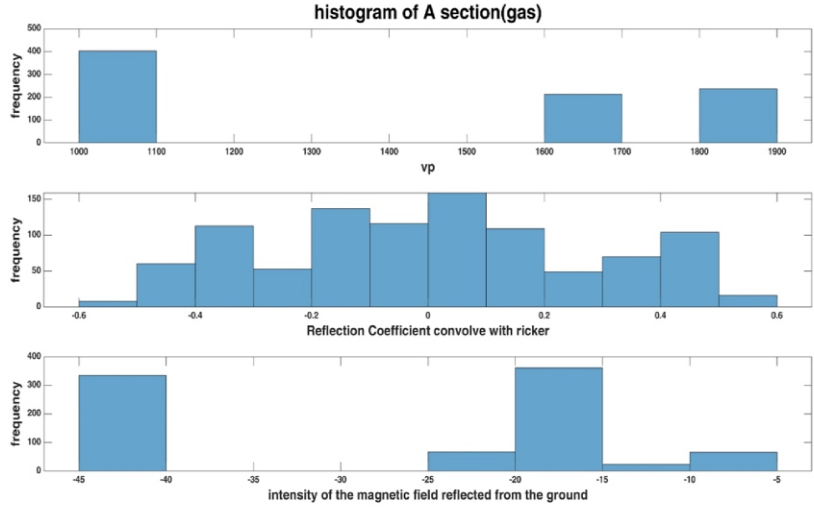

Fig. 7. The histogram diagram related to hydrocarbon range A.

In Fig. 8, the histogram diagram related to hydrocarbon range B is drawn. As we can see in the figure and according to the values of Table 1, the frequency of oil for the figure of the P-wave model is 610, for the figure of the reflection coefficient was convolved with the Ricker wavelet is 115 and in the figure of the intensity of the magnetic field reflected from the ground in the combined method is 420.

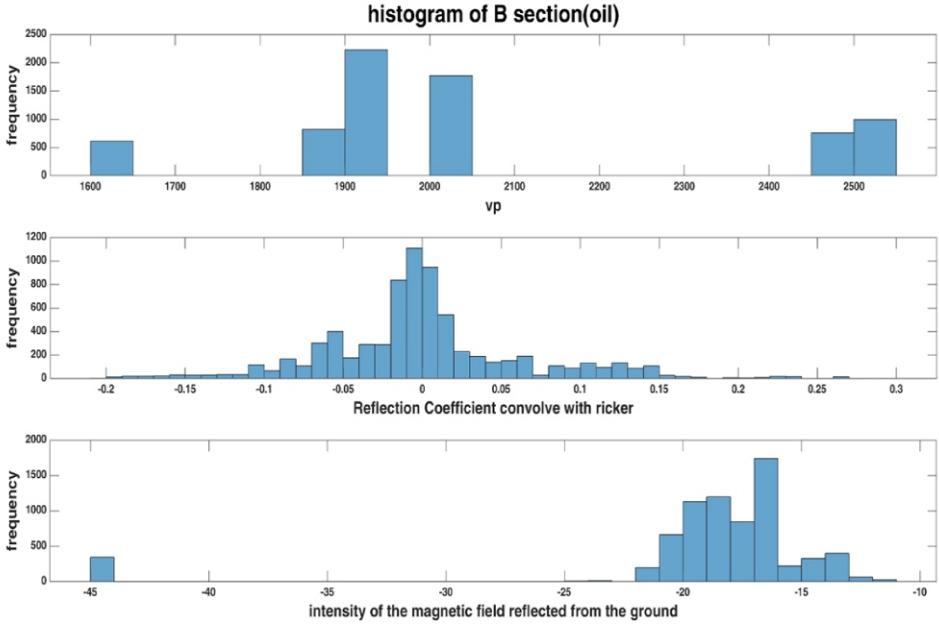

Fig. 8. The histogram diagram related to hydrocarbon range B.

According to these two graphs, we can see that the output of the combined method has obtained the volume of hydrocarbon ranges much more accurately than the seismic method. Also, the location of the ranges is roughly the same as the main location of our synthetic data. But in the seismic method, the locations have been obtained with a displacement of several tens of meters.

CONCLUSIONS

In the Marmousi2 model, units of hydrocarbon were added to the structural model. In Fig. 6, you can see these areas, which are marked as ovals in the figure. By comparing the two Figs. 5 and 6, it can be seen that the model related to the combination of electromagnetic and seismic methods has been well able to identify these areas. Because the amount of resistivity and especially the value of the dielectric coefficient for hydrocarbon sections is significantly different from their host rock. The amount of amplitude of the returned electromagnetic wave from these layers is significantly different from the surrounding layers. This study proved the combination of electromagnetic and seismic methods is an innovative approach to identifying subsurface layers.

ACKNOWLEDGMENTS

The authors would like to acknowledge the Research Council of the University of Tehran. This research did not receive any specific grant from funding agencies in the public, commercial, or not-for-profit sectors.

REFERENCES

Bostani, A., 2020. BEM, Broadband Electromagnetic Smart Method, Phenomenology, Theory, Applications. EAGE Mineral Explorat. Symp., 17-18 September.

Jackson, J.D., 1998. Classical Electrodynamics, 3rd ed., John Wiley & Sons, New York.

Kosloff, D.D. and Baysal, E., 1982. Forward modeling by a Fourier method. Geophysics, 47: 1402-1412.

Martin, G.S., 2004. The Marmousi2 model, elastic synthetic data, and analysis of imaging and AVO in a structurally complex environment. Ph.D. Thesis, University of Houston.

Meju, M.A., Gallardo, L.A. and Mohamed, A.K., 2003. Evidence for correlation of electrical resistivity and seismic velocity in heterogeneous near-surface materials. Geophys. Res. Lett., 30: 1373.

Takougang, E.M.T., Harris, B., Kepic, A. and Le, C.V.A., 2015. Cooperative joint inversion of 3D seismic and magnetotelluric data: With application in a mineral province. Geophysics, 80(4): R175-R187. doi.org/10.1190/GEO2014-0252.1.

Wang, Z., Zhou, C., Zhao, S., Xu, X., Liu, M., Liu, Y., Liao, L. and Shen, X., 2021. Numerical study of global elf electromagnetic wave propagation with respect to lithosphere atmosphere ionosphere coupling, Remote Sens., 13: 4107. https://doi.org/10.3390/rs13204107.